applied sciences

MDPI

Article

Evaluation of Emission Characteristics and Microstructure of Particulate Matters from Excavation and Restoration Work on Asphalt Concrete Pavement

Soohyun Han [1], Jongwon Lee [2] and Cheolmin Baek [2,*]

[1] Department of Civil Engineering, Kyung Hee University, 1732, Deogyeong-daero, Giheung-gu, Yongin-si 17104, Gyeonggi-do, Republic of Korea
[2] Department of Highway and Transportation Research, Korea Institute of Civil Engineering and Building Technology, 283, Goyangdae-ro, Ilsanseo-gu, Goyang-si 10223, Gyeonggi-do, Republic of Korea
* Correspondence: cmbaek@kict.re.kr

Abstract: Road excavation–restoration work, where various construction tasks are performed, may generate large quantities of particulate matter (PM). These PM may accumulate in the surroundings or scatter into the atmosphere, thus affecting the environment and people in the surroundings. This study was conducted as part of a basic research study to reduce scattering PM generated from road excavation–restoration work. This study aimed to investigate the PM_{10} emission trend for each activity of road excavation–restoration work, and to analyze the activity that yields the highest PM_{10} emissions. PM were measured by using a particle spectrometer and the vacuum sweep method, by conducting field (level 1) and chamber experiments (level 2). The PM_{10} emission trends of road-cutting, breaking, removal, excavation, and restoration activities were examined based on field experiments. It was found that the highest PM_{10} emission was generated from road-cutting activities. The road-cutting activities were performed in an enclosed chamber, and the microstructure and the emission characteristics of PM generated by cutting were analyzed. The PM generated during the cutting activity were analyzed by dividing them into scattered and deposited PM. The results showed that as the cutting depth increased, the scattered PM decreased, while the deposited PM tended to increase. Furthermore, as a result of the microstructural analysis of PM conducted during the cutting activity, it was found that the main components were aggregates instead of the components of asphalt binder.

Keywords: excavation–restoration work; particulate matter; asphalt concrete cutting; microstructure

Citation: Han, S.; Lee, J.; Baek, C. Evaluation of Emission Characteristics and Microstructure of Particulate Matters from Excavation and Restoration Work on Asphalt Concrete Pavement. *Appl. Sci.* **2023**, *13*, 323. https://doi.org/10.3390/app13010323

Academic Editors: Dikaia E. Saraga and Thomas Maggos

Received: 11 November 2022
Revised: 22 December 2022
Accepted: 22 December 2022
Published: 27 December 2022

1. Introduction

Particle pollution, also known as particulate matter or PM, is a general term used for a mixture of solid and liquid droplets suspended in the air [1]. PM are classified by their aerodynamic diameters: TSP (total suspended particulate) has a particle diameter of 50 μm or smaller, PM_{10} has a particle diameter of 10 μm or smaller, $PM_{2.5}$ has a particle diameter of 2.5 μm or smaller, and PM_1 has a particle diameter of 1 μm or smaller [2]. The World Health Organization (WHO) has been providing guidelines for PM_{10} and $PM_{2.5}$ since 1987. In 2013, the International Agency for Research on Cancer (IARC), a WHO affiliated organization, classified outdoor air pollution and PM as a carcinogenic agent to humans [3]. The correlations of PM_{10} with various diseases in the respiratory and cardiovascular systems have been confirmed based on various epidemiological studies in which the aerodynamic diameter and particle mass concentration (PMC) are major contribution factors [4–8]. Furthermore, the importance of chemical composition and concentration is emphasized because PM are complexes unlike gaseous pollutants. The elemental components of PM can be used as important basic data for risk assessment of

PM or identification of pollutants because they are associated with large health risks and have characteristics that are preserved without naturally disappearing or changing [9–11].

Construction work is one of the major causes of air pollution in most countries [12–14]. According to the National Fine Dust Information Center of the Ministry of Environment of the Republic of Korea, 48.3% of the total PM_{10} emissions pertained to fugitive dust in 2018; among these, emissions from construction work and resuspended road dust accounted for 61.7% (Figure 1) [15].

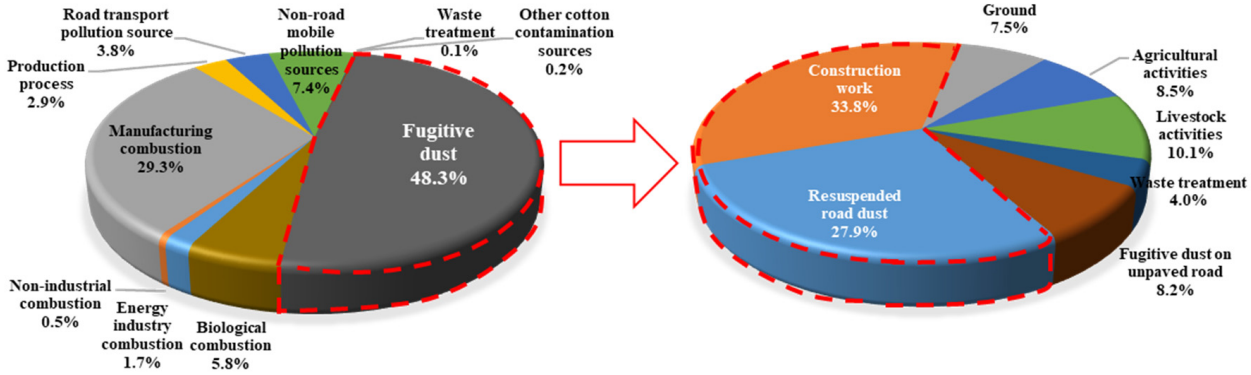

Figure 1. Particulate matter (PM_{10}) emissions as a function of the emission source in Korea (2018).

Road excavation–restoration work involves various construction activities, such as cutting, breaking, excavation, and restoration, and may generate large quantities of PM. The generated PM can accumulate on the road surface or scatter into the atmosphere, thus affecting the air environment, workers, and residents in the surroundings. Moreover, PM accumulated on the road surface are subsequently scattered into the atmosphere by moving vehicles or wind, thus contributing to road-rescattered dust [16–19].

It is expected that road excavation–restoration work will continue to increase owing to the development of urban infrastructures (such as the underground facilities policy) and aged underground facilities. Furthermore, PM generated during road excavation–restoration work does not originate from established emission sources, such as vehicular and nonvehicular exhausts. Little is known about the emissions and composition of these PM [20–24].

Studies on PM emissions from road pavement-related activities (e.g., milling and pavement) are being conducted around the world, and several relevant studies have been published on this subject matter. The PM generated during asphalt concrete paved road-milling activities are reduced by increasing water flow [25]. The average number of particles emitted from asphalt concrete road pavement activities is 1 to 4 times larger than the background concentration. Milling and pavement activities produce very high PM concentrations (PMC) [26]. Asphalt concrete road excavation–restoration work yields high levels of PM_{10} emissions. According to the field measurement performed by Han et. al., the average PMC of PM_{10} generated from road-cutting activities was 1286.3 $\mu g/m^3$, the highest PM_{10} emission among all road excavation–restoration work activities [27]. Asphalt concrete road pavement workers were exposed to high concentrations of ultrafine particles during their work. This may potentially adversely affect their health [28]. Concrete-related work also emits high levels of PM, and concrete-cutting activities yield the highest PM emission levels [29]. Concrete grinding emits high levels of crystalline silica and respirable PM, which can be effectively reduced by applying water flow and local exhaust systems [30]. A summary of the related, previously published studies is given in Table 1.

Table 1. Summary of past studies related to PM emissions from road-paving construction.

Data Type	Activity Type	Instrument Used	Size Range (μm)	Location	Source
PMC	Asphalt milling	Sampling pumps	0.1–10	Outdoor	[25]
PNC	Road works	CPC	0.02–1	Outdoor	[26]
PMC, PNC	Concrete mixing, drilling, cutting	DMA, OPC	0.005–20	Indoor	[29]
PMC	Concrete grinding	Sampling pumps	0.1–10	Indoor	[30]
PMC, PNC	Asphalt works	SMPS, CPC, OPC, OPS	0.014–10	Outdoor	[28]
PMC	Asphalt works	OPC	0.3–35	Outdoor	[27]

Note: PMC, particle mass concentration; PNC, particle number concentration; CPC, condensation particle counter; DMA, differential mobility analyzer; OPC, optical particle counter; SMPS, scanning mobility particle sizer; OPS, optical particle sizer.

This study was conducted as part of a research study which aimed to reduce scattered PM generated in road excavation–restoration work. This study first analyzed the PM_{10} emission trends according to the activities of asphalt concrete road excavation–restoration work based on field experiments (level 1), and the cutting activity yielding the highest PM_{10} emission was then investigated in detail (level 2). The experimental method and results of level 1 are described in Section 2.

In the level 2 experiment, a small, airtight chamber was built, and an experiment was performed in controlled environmental conditions in the chamber. The asphalt concrete-cutting activity was conducted at different cutting depths and conditions. The emission characteristics were analyzed by dividing the PM emitted during the cutting activity into scattered and deposited PM. Furthermore, the microstructures of the emitted PM during these activities were analyzed with the use of scanning electron microscopy (SEM) equipped with an energy dispersive X-ray spectrometer (EDS), and the emitted PM were analyzed based on X-ray diffraction (XRD) analyses.

2. Analysis of PM_{10} Emission Trends through Excavation–Restoration Field Experiment (Level 1)

2.1. Methodology

In order to understand the emission trend of PM generated in excavation and restoration work, an on-site test bed was established and PM emission was measured while performing the same construction method as the actual construction equipment and processes.

The representative PM measurement techniques include the gravimetric analysis, beta-ray absorption, light scattering, and digital image information analysis methods as seen in Table 2 [31–33]. In this study, the light scattering method, which is portable and can be measured in real time, was applied to measure the PM instantaneously generated during construction in the field. For the measurement equipment, the GRIMM's optical particle counter (OPC Model EDM164) was used and this equipment was calibrated according to the ISO 21501-4 standard. This OPC can measure particles in the size range of 0.3–35 μm and measure the PMC of PM_{10} and $PM_{2.5}$. Data was collected and analyzed every 6 s in real time, and the sample flow rate was 1.2 L/min. Thus, it was determined to be suitable for measuring PM generated from road excavation–restoration work.

This experiment set PM_{10} as the main analysis target and five OPCs were used for measurements. Four OPCs were placed 2 m and 4.25 m away from the construction section (the emission source), and the height of the inlet in the OPC was adjusted to 1.5 m. The OPC for measuring background concentration and the automatic weather station (AWS) for collecting meteorological data were placed close to the construction site (Figure 2a). The activities of road excavation–restoration work were classified into road-cutting, breaking, removal, excavation, and restoration, and PM measurement was carried out for the entire process. Two testbeds were built for field testing. Both test beds consisted of a 20 cm thick

asphalt pavement layer and a 60 cm thick subgrade layer. The asphalt concrete layer was applied with a hot mix asphalt most commonly used in urban road pavement. Granite aggregate with a maximum aggregate size of 19 mm and an AP-5 grade asphalt binder were used. The first testbed consisted of six sections and the second testbed consisted of two sections. The size of all sections was the same, and the PM emission amount was measured while repeating the same activities in each section. The average value of each measurement data was used for analysis. The working sections of the first and second field experiments are shown in Figure 2b,c, and the measurement conditions are summarized in Table 3.

Table 2. Characteristics of PM measurement technology.

Characteristics / Method	Portability	Real Time	Accuracy
Gravimetric analysis	X	X	◎
Beta-ray absorption	X	X	◎
Light scattering	○	○	○
Digital image information analysis	○	○	△

Note: ◎, very high; ○, high; △, medium; X, impossible.

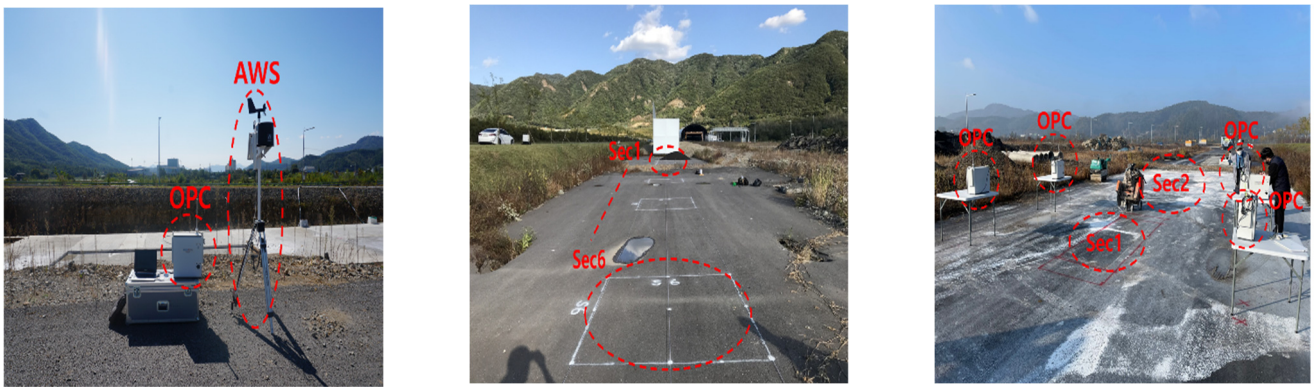

(**a**) (**b**) (**c**)

Figure 2. (**a**) Equipment for collecting background data, (**b**) first field testbed (Sections 1–6), and (**c**) second field testbed (sections 1, 2).

Table 3. Measurement conditions for excavation and restoration work.

Test ID	Data Type	Activity Type	Measuring Equipment	Position from Source (m)	Inlet Height (m)	Number of Sections	Weather Conditions		
							Temp (°C)	Winds (m/s)	Humidity (%)
1	PMC	Asphalt road-cutting, breaking, removal, excavation, restoration	OPC	2, 4.25	1.5	6	18.5	3.3	62.4
2	PMC		OPC	2	1.5	2	16.2	2.7	53.9

2.2. Field Experimental Results and Analysis

This experiment was conducted to identify the PM_{10} emission trends for each activity by performing asphalt concrete road excavation–restoration work, and to select the activity showing the highest level of PM_{10} emission. The PMC of PM_{10} discharged from road excavation–restoration work was measured for road-cutting, breaking, removal, excavation, and restoration activities. Figure 3 shows each activity conducted in the first field experiment and the installation of the OPC to measure PMC can be seen in Figure 3b. The measurement results of two field experiments are summarized in Figure 4. The background concentration was found to be relatively low (10~20 $\mu g/m^3$) compared to PMC generated from excavation–restoration work. The average concentration in Figure 4 shows the result of subtracting the background concentration from the average concentration for each activity.

(**a**) (**b**) (**c**)

(**d**) (**e**) (**f**)

(**g**) (**h**) (**i**)

Figure 3. First field test. (**a**) Cutting, (**b**) breaking, (**c**) removal, (**d**) excavation, (**e**) site sweeping, (**f**) restoration, (**g**) asphalt laying, (**h**) compaction, and (**i**) completed asphalt pavement (Sections 4–6).

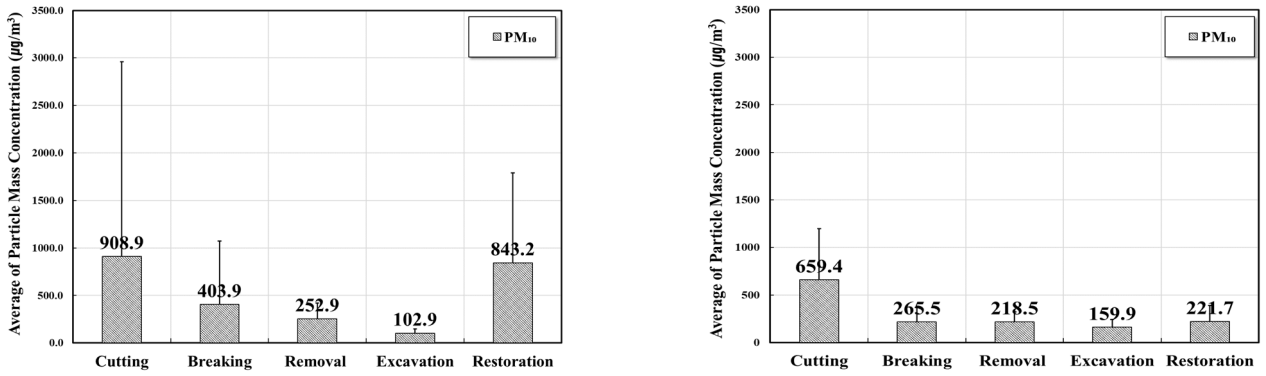

(**a**) (**b**)

Figure 4. PMC for all excavation–restoration work processes: (**a**) First and (**b**) second field test outcomes.

As a result of the first field experiment (Figure 4a), the average PMC of PM_{10} was 908.9 μg/m^3 for road-cutting activity, thus exhibiting the highest PMC among the five activities. It the PMC measured during the restoration work of the first field experiment was considered somewhat high owing to the fact that the workers were carrying stone dust continuously, which was the recovery material around the PM-measuring equipment. The

second experiment (Figure 4b) yielded the highest PMC during the conducted road-cutting activities, which was equal to 659.4 μg/m^3. Based on the PMC analysis and the field observation, it was found that a large quantity of PM was generated immediately after the cutting edge of the cutter touched the pavement surface, when the excavator scratched the road surface, when the excavated soil was loaded on a dump truck, and when the asphalt was laid and compacted.

This experiment could determine and quantify the emission trends of the various road excavation–restoration work activities. Furthermore, it was confirmed that the road-cutting activity exhibited a tendency to emit the highest levels of PM_{10} (based on PMC). This confirmed the same trend as the results of previous studies [26–28]. However, there is a limit to the generalization of the emission characteristics based only on the results of this experiment because these were affected by external factors owing to the nature of the field experiment. Therefore, in the second stage experiment, a small sealed chamber that can minimize external factors was designed and manufactured, and a detailed analysis was conducted on the asphalt concrete-cutting operation showing the highest PM_{10} emission level.

3. Evaluation of PM_{10} Generated in Cutting Operation through Chamber Experiment (Level 2)

3.1. Methodology

3.1.1. Experimental Setup

This experiment was conducted to analyze the microstructure of PM discharged during cutting activities and the characteristics of PM emissions according to the cutting depth. This was achieved by cutting asphalt concrete specimens within a small enclosed chamber.

A small chamber with a size of 2.5 m (B) × 4 m (L) × 2 m (H) was constructed to perform cutting activities in controlled environmental conditions (Figure 5). To collect PM generated in the chamber, an external filter with a pore size of 0.3 μm and an internal filter with a pore size of 10 μm were installed at the rear of the chamber. A HEPA filter was used, and PM_{10} particles collected on the external filter were collected and analyzed. In addition, a fan was installed in the front of the chamber to generate a wind of 3 m/s at the middle position of chamber in order to collect the PM scattered inside the chamber by the filter at the rear.

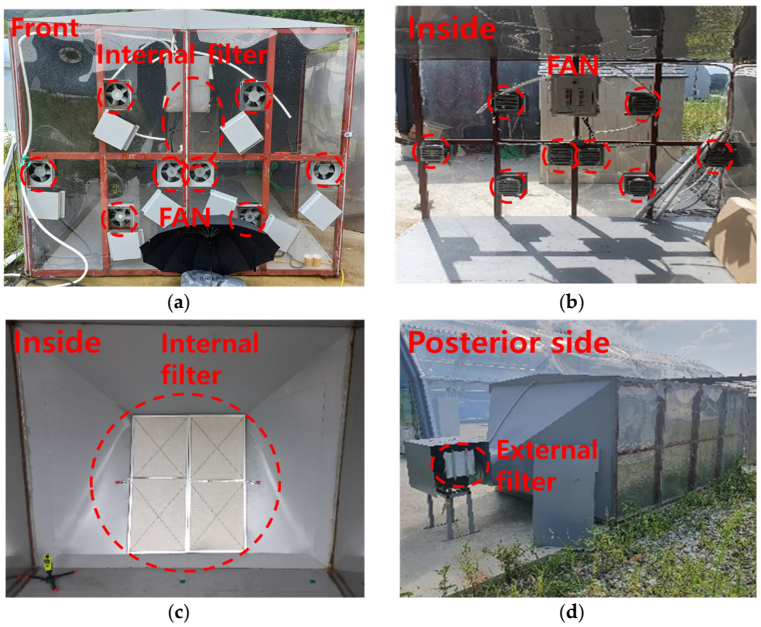

Figure 5. Enclosed chamber. (**a**) Front view, (**b**) fan, (**c**) internal filter, and (**d**) external filter.

The asphalt concrete specimen in Figure 6a was fabricated to simulate the asphalt concrete road. The materials used for the asphalt concrete specimen were granite aggregate and AP-5 asphalt binder, which are commonly used in urban road pavements. The specimens were fabricated to have a size of 1000 mm × 1000 mm × 250 mm considering the size of the chamber, the operating range of the small cutter, and the cutting depth.

(**a**) (**b**)

Figure 6. (**a**) Preparation of asphalt concrete specimen and (**b**) chamber experimental setup.

The cutter used in the experiment was the equipment commonly used for small-scale road-cutting work. The maximum cutting depth is 150 mm, and dry cutting and wet cutting are possible. The experiment was conducted after placing the asphalt concrete specimen and cutter inside the chamber, as shown in Figure 6b.

3.1.2. Experimental Method

In this study, asphalt concrete specimen cutting activity was performed in four conditions, as shown in Table 4. The cutting length of all experiments was fixed at 800 mm. In the cases of the test identities (IDs) 1–3, the cutting depths were set to 50 mm, 70 mm, and 100 mm, respectively, to analyze the PM emission characteristics according to the cutting depth. In the cases of test IDs 3 and 4, the cutting depth and cutting length were set to be the same, and the PM emission characteristics according to the cutting conditions were analyzed by performing dry and wet cutting.

Table 4. Experimental conditions.

Test ID	Depth (mm)	Length (mm)	Condition	Cut Area (m^2)
1	50	800	Dry	0.04
2	70	800	Dry	0.056
3	100	800	Dry	0.08
4	100	800	Wet	0.08

PM generated from cutting activities were analyzed by dividing them into scattered and deposited PM. The scattered PM were analyzed by using the filter installed in the chamber and GRIMM's OPC. The OPC used in this experiment is the same equipment used in Section 2. The OPC calculated the mass concentration by measuring the number concentration and applying a correction factor considering the density of the particles to be measured. The correction factor was calculated by measuring the density of the particles collected in the low-volume sampler attached to the OPC [34].

The deposited PM was analyzed by using the vacuum sweep method, which is a road dust measurement method suggested by the US-EPA [35]. The vacuum sweep method collects silt accumulated on the paved road surface by using a vacuum cleaner, measures the weight of the silt by using sieve analysis, and divides this by the sampled road area to calculate the silt loading. Silt loading (sL) refers to the weight of piled up silt with a geometric diameter $\leq$75 μm per unit road area, which indicates the rescattering potential

of road dust. In this study, the vacuum sweep method was used to analyze the residual, rescattered PM after cutting the asphalt road pavement, and was calculated as follows. (1) After the cutting activity was finished, the PM present in the chamber and specimens was collected using an industrial vacuum cleaner. (2) The collected PM was sieved. The sL was calculated by dividing the weight of the silt that has passed through a 200-mesh sieve by the cutting area of the asphalt specimen. The deposited PM was analyzed using this method.

SEM/EDS (Merlin Compact, Carl Zeiss, Jena, Germany) and XRD (Bruker-AXS, Shibuya, Tokyo, Japan) analyses were performed to analyze information, such as shape, particle size, and chemical composition of the PM generated from the asphalt concrete-cutting activity. Elemental components, such as C, O, Na, Mg, Al, Si, S, Cl, K, Ca, Ti, V, Cr, Mn, Cu, Fe, Ni, and Zn, were analyzed by EDS at specified SEM analysis conditions at an acceleration voltage of 15 kV and a working distance (WD) of 10 mm, while adjusting the magnification according to the sample to be analyzed. Furthermore, the analyzed sample was coated with Pt to increase the accuracy of the analysis. The content of the elements analyzed by EDS was expressed in weight %.

3.2. Experimental Results and Analysis

3.2.1. Scattered PM

The emission characteristics of scattered PM_{10} generated from the asphalt concrete specimen-cutting activity were analyzed by measuring PM using the OPC. The generation process of scattered PM_{10} from the asphalt concrete specimen-cutting activities was similar for test IDs 1–4. The PMC and particle number concentration (PNC) of the test ID 1 are shown in Figure 7.

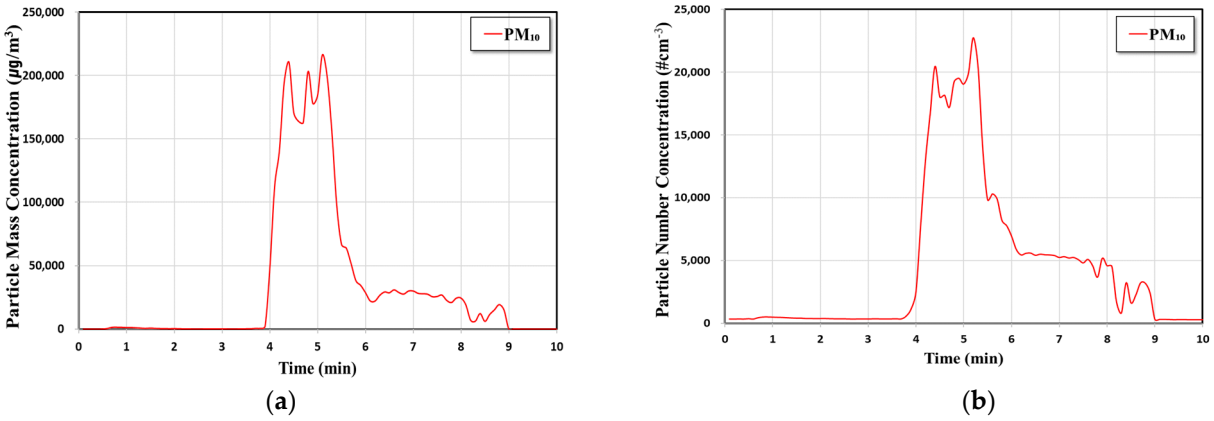

Figure 7. Scattered dust during cutting (test ID 1). (**a**) PMC and (**b**) PNC.

The measurement of test ID 1 took approximately 10 min, and the cutting activity was performed for approximately 2 min (from 4 to 6 min). In all experiments, PMC and PNC showed a sharp increase immediately after the cutting blade touched the cutting surface. In addition, the dust settled in approximately 2 to 3 min after the work was finished. In all tests, the trends of PMC and PNC were found to be similar. Table 5 shows the average PMCs of PM_{10}, $PM_{2.5}$, and PM_1 according to the cutting depth.

Table 5. Average PMC values according to cutting depth.

Test ID	Depth (mm)	PM_{10} (μg/m^3)	$PM_{2.5}$ (μg/m^3)	PM_1 (μg/m^3)
1 (dry)	50	38,069.43	4669.73	588.71
2 (dry)	70	24,894.83	3139.14	369.41
3 (dry)	100	18,475.79	1455.27	147.91
4 (wet)	100	1713.62	427.14	67.48

First, as a result of testing in dry states, the scattered PM_{10} decreased as the cutting depth increased. In the case of test ID 1 (depth 50 mm), PM_{10}, PM $_{2.5}$, and PM_1 yielded PMCs which were approximately 2.1-, 3.2-, and 4-times higher compared with that for test ID 3 (depth 100 mm), respectively. As the cutting depth increased, the scattered PM_{10} decreased because the dust was trapped inside the asphalt specimen. In the case of test ID 4 where wet cutting was performed, the PMC of scattered PM_{10} decreased by approximately 90.7% compared with test ID 3 where dry cutting was performed under the same conditions.

The particle number distribution (PND) was analyzed to determine the number of particles (based on their sizes) generated from the cutting activities for PM with sizes in the range of 0.3–35 µm. The variations of PNDs as a function of the cutting depth are shown in Figure 8. In test IDs 1–4, the proportions of PM_1 were 83.1%, 76.7%, 73.9%, and 84.5%, respectively, thus indicating that PM_1 occupies a large proportion of the total PNC. Moreover, it was found that the particle number of generated PM decreased as the cutting depth increased in every range of particle size.

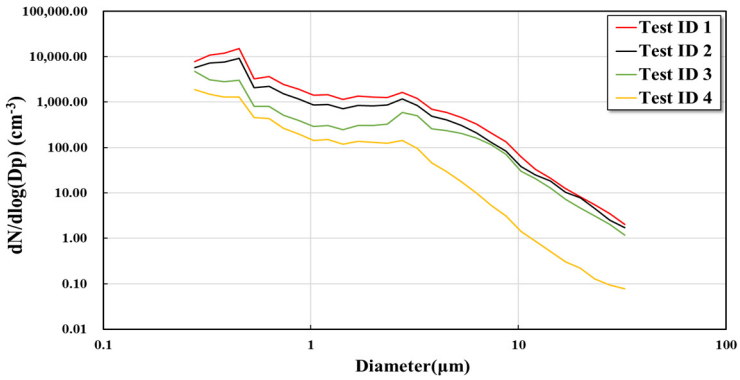

Figure 8. Particle number distribution as a function of diameter at different cutting depths.

As a result of analyzing the OPC measurements, it was found that as the cutting depth increased, not only the particle concentration but also the number of particles scattered due to the cutting activities decreased.

The weights of PM collected in the 10 µm internal filter and the 0.3 µm external filter were measured. The results are listed in Table 6. The weight of PM collected in the filter decreased as a function of the cutting depth. The weights of PM obtained by wet cutting decreased by approximately 93.2% compared with that produced by dry cutting. The analyzed results of PM collected in the filter show the same trend as the mass concentration and number of particles analyzed by the OPC.

Table 6. Weight of PM captured by the filter.

Test ID	PM of Internal Filter (g)	PM of External Filter (g)	Total PM (g)
1 (dry)	5.31	17.53	22.84
2 (dry)	1.38	15.27	16.65
3 (dry)	1.34	14.88	16.22
4 (wet)	0.23	0.88	1.11

3.2.2. Deposited PM

The characteristics of deposited PM generated from the asphalt concrete specimen were analyzed by measuring silt loading. The results are shown in Table 7. First, as a result of testing for each cutting depth in the dry state, the quantity of deposited PM increased as a function of the cutting depth. The highest quantity of PM was generated from the asphalt concrete specimen-cutting activity when the cutting blade contacted the specimen at the time at which the cutting activity started. At this time, the scattered PM generated on the surface yielded the highest peak in the previous section. Subsequently, the deposited PM

increased as cutting progressed. This suggests that the deposited PM on the surface of the asphalt concrete specimen increased as a function of the cutting depth.

Table 7. Comparison of silt loading values associated with cutting activities.

Test ID	Collected PM (g)	Silt (g)	Cut Area (m^2)	sL (g/m^2)
1 (dry)	200	35.19	0.04	879.79
2 (dry)	323	64.31	0.056	1148.39
3 (dry)	442	96.97	0.08	1212.14
4 (wet)	560	133.08	0.08	1663.44

In the case of Test ID 4 in which wet cutting was performed, the PMC of scattered PM_{10} decreased by more than 90%, as shown in the analysis in the previous section, but the deposited PM tended to increase by approximately $\geq$37% as a result of the sL analysis. As a result of the silt measurement, the deposited PM generated from the cutting activity tended to increase as a function of the cutting depth, and increased further in the case of wet cutting.

The ratio of deposited and scattered PM was verified by the total PM collected from the filter in Table 6 and the total PM collected from the chamber and specimen in Table 7. In Test IDs 1–4, the ratios of scattered PM to deposited PM were 10.25%, 4.90%, 3.54%, and 0.20%, respectively. Thus, the proportion of scattered PM tended to decrease as the cutting depth increased.

The particle size of the deposited PM was analyzed using a particle size analyzer (HELOS 5145C, RODOS T4.1) which can measure in the range of 0.5–875 µm. The particle size analysis results for each sample are shown in Figure 9. In the case of test IDs 1 and 2, the ratios of particle sizes below PM_{10} were 24.08% and 26.04%, respectively. Moreover, it was found that most of the particles had sizes in the range of 10–100 µm. Meanwhile, the ratios of particle size below PM_{10} of Test IDs 3 and 4 were 36.55% and 37.74%, respectively. Unlike test IDs 1 and 2, most of the particles had sizes which were in the range of 10–20 µm. Similar to the previous OPC analysis results, as the cutting depth increased, PM_{10} trapped inside the asphalt specimen increased and it can be seen that such PM_{10} is included in the deposited PM.

3.2.3. SEM Analysis

The characteristics of PM generated from the asphalt concrete specimen-cutting activities were analyzed using SEM and EDS. Figure 10a,b show SEM images of PM generated from the asphalt concrete specimen cutting-activities at 200× and 1000× magnifications. Furthermore, Figure 10c,d show the EDS elemental map which is the surface analysis outcomes for each element and the EDS spectrum, respectively.

In the SEM image analysis, individual particles of various shapes and sizes ranging from several to tens of µm appeared in the PM. In addition, as a result of analysis with increased magnification, it was found that the tens of µm particles were formed due to the combination of several µm particles.

Particles with typical characteristics among the observed images were classified into three types, and the analysis results are presented in Table 8. In the case of Type-1, C and O components were found to constitute 65.8% of the total. This is a carbon compound, which is a major component of the asphalt binder, and it can be seen that Type-1 is PM mainly containing the asphalt binder. Type 2 was composed of large quantities of O and Si which accounted for 77.5% of the total. These are quartz particles and are considered to be the aggregate part of the asphalt concrete specimen [36]. Unlike the above two types, Type 3 was composed of C, O, Al, Si, Mg, and various amounts of Na, S, and K. Accordingly, this type can be composed of Al-Si-O, Ca-Al-Si-O, Fe-Al-Si-O, K-Al-Si-O, Ti-Al-Si-O, and other compounds. They are considered to be aluminosilicate minerals that can be found in nature [37,38]. Furthermore, if the contents of Ca in the above components are slightly

increased, these components could be detected as $CaCO_3$ composed of Ca-C-O, Ca-S-O, Ca-Si-Fe-Mg-O, and other compounds [39].

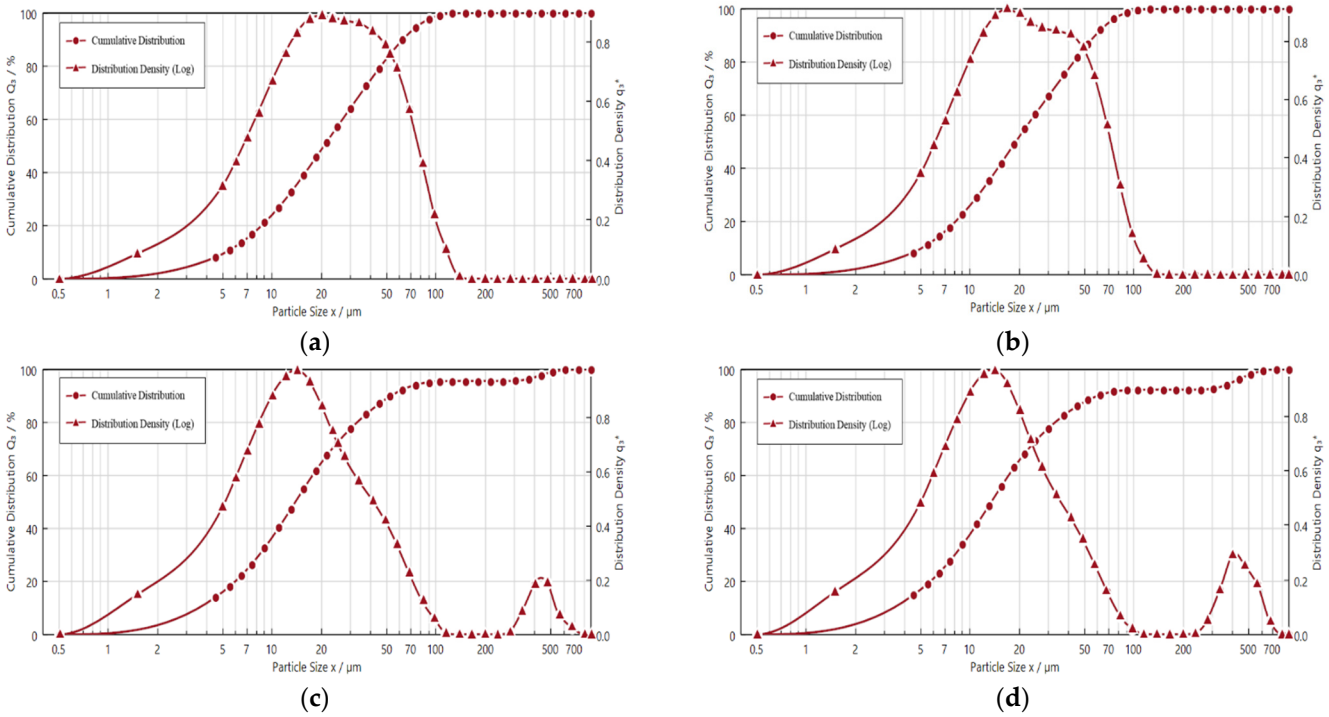

Figure 9. Particle size distribution of deposited PM; Test IDs (**a**) 1, (**b**) 2, (**c**) 3, and (**d**) 4.

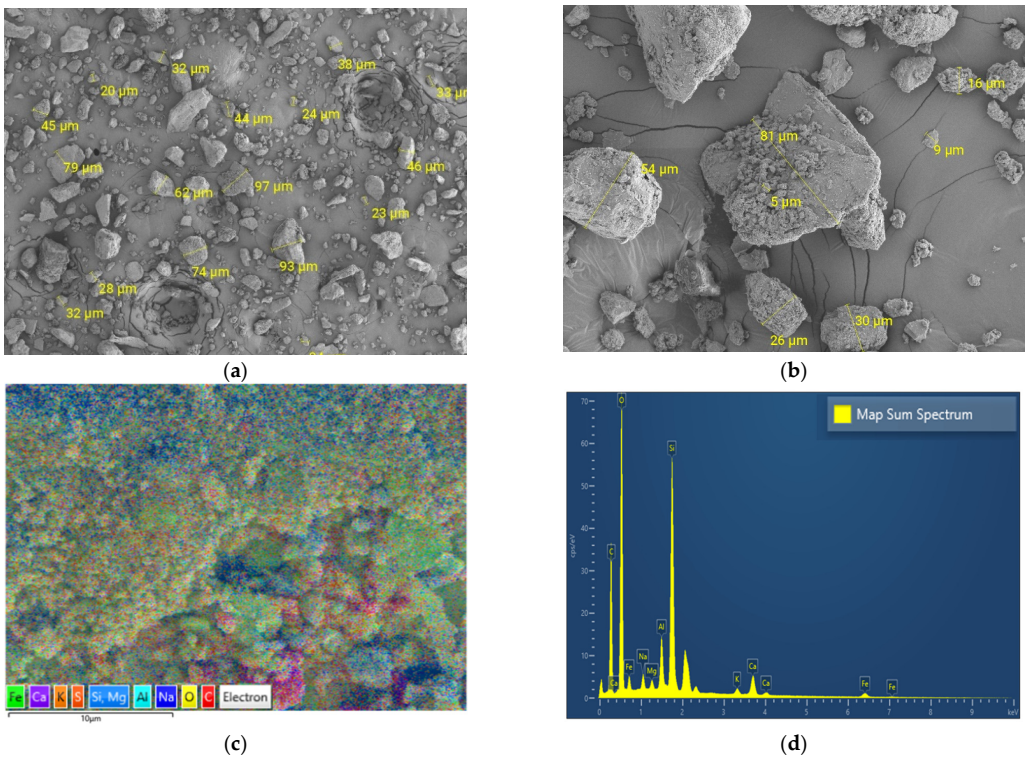

Figure 10. Scanning electron microscopy (SEM) image and energy dispersive X-ray spectroscopy (EDS) mapping analysis of PM. (**a**) SEM image of PM (200×), (**b**) SEM image of PM (1000×), (**c**) EDS elemental mapping, and (**d**) spectrum obtained by EDS.

Table 8. Elemental composition by average weight (%) from mapping analysis.

Sample	Weight (%)										
	C	O	Na	Mg	Al	Si	S	K	Ca	Ti	Fe
Type 1	30.2	35.6	0.96	0.53	3.18	15.8	0.48	1.16	4.9	0.7	6.49
Type 2	6.46	49.6	2.88	-	8.43	27.9	-	0.73	3.20	-	0.80
Type 3	12.9	39.4	2.66	6.25	10.9	15.4	0.28	0.62	5.97	0.4	5.22

The result of SEM and EDS analyses showed that three types of PM were generated during the cutting process of the asphalt concrete specimen. It was found that PM produced included mainly type 2 and type 3 PM. This is because the composition of the asphalt concrete specimen is generally 95% aggregate and 5% asphalt binder.

3.2.4. XRD Analysis

The characteristics of the PM generated from the asphalt concrete specimen-cutting activity were analyzed by using XRD. As a result of the XRD analysis, the main peaks were SiO_2 and $CaCO_3$ of the crystalline material due to the aggregate component, and it was found that many residual peaks of crystalline minerals combined with a large amount of elements such as Ca, Si, O, Al, Mg were also found (Figure 11).

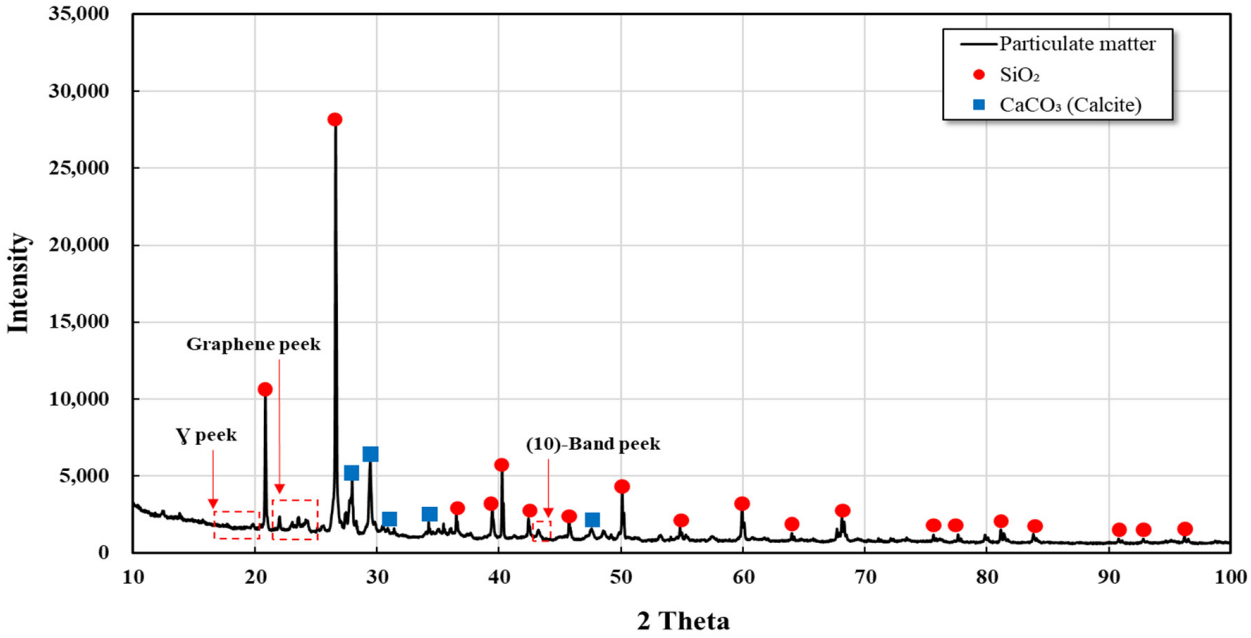

Figure 11. X-ray diffraction analysis of PM obtained from asphalt concrete cutting.

The asphalt binder is composed of amorphous materials unlike aggregates. The XRD pattern of asphalt consists of four major peaks: γ -peak, (002)-graphene peak, (10)-band, and (11)-band. The peaks of pure asphalt and mixtures appear near the 2θ values in the range of 20–25°. The resulting γ-peak originated from the X-rays scattered by aliphatic chains or condensed naphthenic rings. It has been reported that these peaks were mainly derived from paraffin [40]. The (002)-graphene peak at 2θ values is caused by the X-ray diffraction of the aromatic sheet. The (10)- and (11)-band peaks are also expressed as (100) and (110). They appear because of the structure of the aromatic molecule in the plane. They represent the first and second elements in the ring compound.

Among the four asphalt peaks, the peak mainly observed in the PM was the (002)-graphene peak. The γ-peak also appeared, although its intensity was small. Mean-

while, the (10) and (11) peaks were not verified owing to the very low strength of the aromatic sheet [41].

The results of XRD analysis of the PM generated from the asphalt concrete specimen cutting-activity showed that the main components of the aggregates were detected more easily than the components of the asphalt binder. Furthermore, a similar trend to the SEM and EDS analysis results presented in the previous section was observed.

4. Conclusions

This study was conducted as part of a basic research study executed to reduce scattered PM generated from road excavation–restoration work. The PM_{10} emission trend for each excavation–restoration work activity was identified and the PM emission characteristics were analyzed according to the PM microstructure and cutting depth during asphalt concrete cutting activities. The major findings of this study are outlined below.

As a result of measuring the PMC of scattered PM_{10} in the road excavation–restoration work, it was found that large quantities of PM were generated immediately after the cutting blade of the cutter touched the surface, when the ground was vibrated by the breaker, when the excavator scraped the road surface, when the excavated soil was loaded onto a dump truck, and when the asphalt was poured and compacted. Furthermore, the road-cutting activity showed a tendency to emit the largest PM_{10} quantities.

The asphalt concrete specimen cutting-activity was performed in a small, enclosed chamber. During the cutting activity, the PNC and PMC of PM_{10} rapidly increased immediately after the cutting blade touched the cutting surface. As a result of the analysis of scattered PM, the PMC of scattered PM_{10} generated from the cutting activity tended to decrease as the cutting depth increased. Moreover, the number of particles exhibited the same trend.

The analyzed results of the deposited PM showed that the deposited PM increased as a function of the cutting depth. In the case of wet cutting, the PMC of scattered PM_{10} decreased by approximately 90.7% compared with dry cutting, but the deposited PM increased by approximately 37%. The ratios of PM collected on the filter compared with the deposited PM were 10.25%, 4.90%, 3.54%, and 0.20%. Thus, the ratios of scattered PM decreased as the cutting depth increased. This finding is related to the analyzed results of scattered PM. The deeper the cutting depth is, the larger the space inside the cut surface and in the voids in the asphalt specimen wherein PM can reside. As a result, scattered PM decreased and deposited PM increased.

As a result of the SEM and EDS analyses, three types of PM were found to be generated from the asphalt concrete specimen-cutting activities. Type-1 PM are considered to be carbon compounds, and are mainly composed of asphalt binder. Type-2 PM are considered to be quartz particles from the aggregate part of the asphalt concrete specimen. Type-3 PM, unlike the above two types, are composed of C, O, Al, Si, and Mg, and Na, S, and K were also detected in various quantities. They can be composed of Al-Si-O, Ca-Al-Si-O, Fe-Al-Si-O, K-Al-Si-O, and Ti-Al-Si-O, and may also contain other similar compounds. Thus, they are considered to be naturally occurring aluminosilicate minerals.

The XRD analysis results of the PM generated from the asphalt concrete specimen-cutting activity showed that the main components of the aggregate were detected rather than the components of the asphalt binder. This suggests a trend similar to those observed in the SEM and EDS analysis outcomes.

Author Contributions: Data curation, S.H. and J.L.; Writing—original draft, S.H. and J.L.; Writing—review & editing, C.B.; Supervision, C.B. All authors have read and agreed to the published version of the manuscript.

Funding: This work was supported by the Korea Agency for Infrastructure Technology Advancement (KAIA) grant funded by the Ministry of Land, Infrastructure, and Transport (Grant No. 22POQW-B152342-01).

Institutional Review Board Statement: Not applicable.

Informed Consent Statement: Not applicable.

Data Availability Statement: Data available in a publicly accessible repository.

Conflicts of Interest: The authors declare no conflict of interest.

References

1. EPA. Particulate Matter (PM) Pollution. 2021. Available online: https://www.epa.gov/pm-pollution (accessed on 17 January 2022).
2. Ministry of Environment of Korea. Fugitive Dust Management Manual. Available online: www.me.go.kr (accessed on 12 January 2022).
3. Loomis, D.; Grosse, Y.; Lauby-Secretan, B.; El Ghissassi, F.; Bouvard, V.; Benbrahim-Tallaa, L.; Guha, N.; Baan, R.; Mattock, H.; Straif, K. The carcinogenicity of outdoor air pollution. *Lancet Oncol.* **2013**, *14*, 1262–1263. [CrossRef]
4. Pope, C.A., III; Dockery, D.W. Health Effects of Fine Particulate Air Pollution: Lines that Connect. *J. Air Waste Manag. Assoc.* **2006**, *56*, 709–742. [CrossRef] [PubMed]
5. Brunekreef, B.; Forsberg, B. Epidemiological evidence of effects of coarse airborne particles on health. *Eur. Respir. J.* **2005**, *26*, 309–318. [CrossRef] [PubMed]
6. Heal, M.R.; Kumar, P.; Harrison, R.M. Particles, air quality, policy and health. *Chem. Soc. Rev.* **2012**, *41*, 6606–6630. [CrossRef] [PubMed]
7. Brown, J.S.; Gordon, T.; Price, O.; Asgharian, B. Thoracic and respirable particle definitions for human health risk assessment. *Part. Fibre Toxicol.* **2013**, *10*, 12. [CrossRef]
8. Thén, W.; Salma, I. Particle Number Concentration: A Case Study for Air Quality Monitoring. *Atmosphere* **2022**, *13*, 570. [CrossRef]
9. Kang, C.-H.; Hu, C.-G. Characteristics of the Number and the Mass Concentrations and the Elemental Compositions of PM10in Jeju Area. *J. Environ. Sci.* **2014**, *23*, 447–457. [CrossRef]
10. Zhang, R.; Han, Z.; Shen, Z.; Cao, J. Continuous measurement of number concentrations and elemental composition of aerosol particles for a dust storm event in Beijing. *Adv. Atmos. Sci.* **2008**, *25*, 89–95. [CrossRef]
11. Na, D.J.; Lee, B.K. A study on the characteristics of PM10 and air-borne metallic elements produced in the industrial city. *J. Korean Soc. Atmos. Environ.* **2000**, *16*, 23–35.
12. Cheriyan, D.; Choi, J.-H. A review of research on particulate matter pollution in the construction industry. *J. Clean. Prod.* **2020**, *254*, 120077. [CrossRef]
13. Choi, J. *Monitoring Particulate Matter Emission from Construction Activity Which Causes Long-Term Health Issues and Premature Deaths*; CIB World Building Congress: Hong Kong, SAR, China, 2019; p. 8.
14. Li, C.Z.; Zhao, Y.; Xu, X. Investigation of dust exposure and control practices in the construction industry: Implications for cleaner production. *J. Clean. Prod.* **2019**, *227*, 810–824. [CrossRef]
15. National Center for Fine Dust Information of Korea. Statistics on Air Pollutant Emissions in 2018. Available online: www.air.go.kr (accessed on 17 January 2022).
16. Faber, P.; Drewnick, F.; Borrmann, S. Aerosol particle and trace gas emissions from earthworks, road construction, and asphalt paving in Germany: Emission factors and influence on local air quality. *Atmos. Environ.* **2015**, *122*, 662–671. [CrossRef]
17. Air Quality Expert Group (AQEG)-Defra. Non-Exhaust Emissions from Road Traffic. 2019. Available online: https://uk-air.defra.gov.uk/ (accessed on 15 January 2022).
18. Jancsek-Turóczi, B.; Hoffer, A.; Nyírő-Kósa, I.; Gelencsér, A. Sampling and characterization of resuspended and respirable road dust. *J. Aerosol Sci.* **2013**, *65*, 69–76. [CrossRef]
19. Tervahattu, H.; Kupiainen, K.J.; Räisänen, M.; Mäkelä, T.; Hillamo, R. Generation of urban road dust from anti-skid and asphalt concrete aggregates. *J. Hazard. Mater.* **2006**, *132*, 39–46. [CrossRef] [PubMed]
20. Kumar, P.; Robins, A.; Vardoulakis, S.; Britter, R. A review of the characteristics of nanoparticles in the urban atmosphere and the prospects for developing regulatory controls. *Atmos. Environ.* **2010**, *44*, 5035–5052. [CrossRef]
21. Charron, A.; Harrison, R.M. Primary particle formation from vehicle emissions during exhaust dilution in the roadside atmosphere. *Atmos. Environ.* **2003**, *37*, 4109–4119. [CrossRef]
22. Dall'Osto, M.; Thorpe, A.; Beddows, D.C.S.; Harrison, R.M.; Barlow, J.F.; Dunbar, T.; Williams, P.I.; Coe, H. Remarkable dynamics of nanoparticles in the urban atmosphere. *Atmos. Chem. Phys.* **2011**, *11*, 6623–6637. [CrossRef]
23. Han, S.; Youn, J.-S.; Jung, Y.-W. Characterization of PM10 and PM2.5 source profiles for resuspended road dust collected using mobile sampling methodology. *Atmos. Environ.* **2011**, *45*, 3343–3351. [CrossRef]
24. Abu-Allaban, M.; Gillies, J.A.; Gertler, A.W.; Clayton, R.; Proffitt, D. Tailpipe, resuspended road dust, and brake-wear emission factors from on-road vehicles. *Atmos. Environ.* **2003**, *37*, 5283–5293. [CrossRef]
25. National Institute for Occupational Safety and Health (NIOSH). *In Depth Survey of Dust Control Technology for Asphalt Milling*; National Institute for Occupational Safety and Health (NIOSH): Cincinnati, OH, USA, 2007.
26. Freund, A.; Zuckerman, N.; Baum, L.; Milek, D. Submicron particle monitoring of paving and related road construction operations. *J. Occup. Environ. Hyg.* **2012**, *9*, 298–307. [CrossRef]
27. Han, S.H.; Yang, S.L.; Lee, J.W.; Baek, C.M. Evaluation of fugitive dust emission generated by the construction process of pavement excavation–restoration through the field test. *J. Korean Soc. Road Eng.* **2020**, *22*, 61–68. [CrossRef]
28. Elihn, K.; Ulvestad, B.; Hetland, S.; Wallén, A.; Randem, B.G. Exposure to Ultrafine Particles in Asphalt Work. *J. Occup. Environ. Hyg.* **2008**, *5*, 771–779. [CrossRef] [PubMed]

29. Azarmi, F.; Kumar, P.; Mulheron, M. The exposure to coarse, fine and ultrafine particle emissions from concrete mixing, drilling and cutting activities. *J. Hazard. Mater.* **2014**, *279*, 268–279. [CrossRef] [PubMed]
30. Akbar-Khanzadeh, F.; Milz, S.; Ames, A.; Susi, P.P.; Bisesi, M.; Khuder, S.A.; Akbar-Khanzadeh, M. Crystalline Silica Dust and Respirable Particulate Matter During Indoor Concrete Grinding—Wet Grinding and Ventilated Grinding Compared with Uncontrolled Conventional Grinding. *J. Occup. Environ. Hyg.* **2007**, *4*, 770–779. [CrossRef]
31. Yang, J.H.; Tae, S.H.; Lee, K.S. Basic Study on the Measurement of Finedust Based on Light Scattering Method in Construction Site. In Proceedings of the Annual Conference of the Architectural Institute of Korea, Architectural Institute of Korea, Seoul, Republic of Korea, 20–26 September 2019; Volume 39, pp. 476–479.
32. Im, S.; Yu, J. Analysis of fugitive dust measurement technique for fugitive dust management in construction site. *Proc. Korean Inst. Archit. Spring* **2018**, *38*, 672–673.
33. Choi, S.I.; An, J.; Jo, Y.M. Review of analysis principle of fine dust. *KCI News* **2018**, *21*, 16–23.
34. Singh, G.K.; Choudhary, V.; Gupta, T.; Paul, D. Investigation of size distribution and mass characteristics of ambient aerosols and their combustion sources during post-monsoon in northern India. *Atmos. Pollut. Res.* **2019**, *11*, 170–178. [CrossRef]
35. EPA. AP 42, Air Emission Factors and Quantification. Miscellaneous Sources, 13.2.1 Paved Roads. Available online: www.epa.gov/air-emissions-factors-and-quantification/ap-42-fifth-edition-volume-i-chapter-13-miscellaneous-0 (accessed on 17 January 2022).
36. Pachauri, T.; Singla, V.; Satsangi, A.; Lakhani, A.; Kumari, K.M. SEM-EDX Characterization of Individual Coarse Particles in Agra, India. *Aerosol Air Qual. Res.* **2013**, *13*, 523–536. [CrossRef]
37. Satsangi, P.G.; Yadav, S. Characterization of PM2. 5 by X-ray diffraction and scanning electron microscopy–energy dispersive spectrometer: Its relation with different pollution sources. *Int. J. Environ. Sci. Technol.* **2014**, *11*, 217–232. [CrossRef]
38. Byeon, S.-H.; Willis, R.; Peters, T.M. Chemical Characterization of Outdoor and Subway Fine (PM2.5–1.0) and Coarse (PM10–2.5) Particulate Matter in Seoul (Korea) by Computer-Controlled Scanning Electron Microscopy (CCSEM). *Int. J. Environ. Res. Public Health* **2015**, *12*, 2090–2104. [CrossRef]
39. Lough, G.C.; Schauer, J.J.; Park, J.-S.; Shafer, M.M.; DeMinter, J.T.; Weinstein, J.P. Emissions of Metals Associated with Motor Vehicle Roadways. *Environ. Sci. Technol.* **2004**, *39*, 826–836. [CrossRef] [PubMed]
40. Siddiqui, M.N.; Ali, M.F.; Shirokoff, J. Use of X-ray diffraction in assessing the aging pattern of asphalt fractions. *Fuel* **2002**, *81*, 51–58. [CrossRef]
41. AlHumaidan, F.S.; Hauser, A.; Rana, M.S.; Lababidi, H.M.; Behbehani, M. Changes in asphaltene structure during thermal cracking of residual oils: XRD study. *Fuel* **2015**, *150*, 558–564. [CrossRef]